Precision measurement of the matrix elements
for $\eta \to \pi^+\pi^-\pi^0$ and $\eta \to \pi^0\pi^0\pi^0$ decays

M. Ablikim,[1] M. N. Achasov,[13,b] P. Adlarson,[73] R. Aliberti,[34] A. Amoroso,[72a,72c] M. R. An,[38] Q. An,[69,56] Y. Bai,[55] O. Bakina,[35] I. Balossino,[29a] Y. Ban,[45,g] V. Batozskaya,[1,43] K. Begzsuren,[31] N. Berger,[34] M. Berlowski,[43] M. Bertani,[28a] D. Bettoni,[29a] F. Bianchi,[72a,72c] E. Bianco,[72a,72c] J. Bloms,[66] A. Bortone,[72a,72c] I. Boyko,[35] R. A. Briere,[5] A. Brueggemann,[66] H. Cai,[74] X. Cai,[1,56] A. Calcaterra,[28a] G. F. Cao,[1,61] N. Cao,[1,61] S. A. Cetin,[60a] J. F. Chang,[1,56] T. T. Chang,[75] W. L. Chang,[1,61] G. R. Che,[42] G. Chelkov,[35,a] C. Chen,[42] Chao Chen,[53] G. Chen,[1] H. S. Chen,[1,61] M. L. Chen,[1,56,61] S. J. Chen,[41] S. M. Chen,[59] T. Chen,[1,61] X. R. Chen,[30,61] X. T. Chen,[1,61] Y. B. Chen,[1,56] Y. Q. Chen,[33] Z. J. Chen,[25,h] W. S. Cheng,[72c] S. K. Choi,[10] X. Chu,[42] G. Cibinetto,[29a] S. C. Coen,[4] F. Cossio,[72c] J. J. Cui,[48] H. L. Dai,[1,56] J. P. Dai,[77] A. Dbeyssi,[19] R. E. de Boer,[4] D. Dedovich,[35] Z. Y. Deng,[1] A. Denig,[34] I. Denysenko,[35] M. Destefanis,[72a,72c] F. De Mori,[72a,72c] B. Ding,[64,1] X. X. Ding,[45,g] Y. Ding,[33] Y. Ding,[39] J. Dong,[1,56] L. Y. Dong,[1,61] M. Y. Dong,[1,56,61] X. Dong,[74] S. X. Du,[79] Z. H. Duan,[41] P. Egorov,[35,a] Y. L. Fan,[74] J. Fang,[1,56] S. S. Fang,[1,61] W. X. Fang,[1] Y. Fang,[1] R. Farinelli,[29a] L. Fava,[72b,72c] F. Feldbauer,[4] G. Felici,[28a] C. Q. Feng,[69,56] J. H. Feng,[57] K. Fischer,[67] M. Fritsch,[4] C. Fritzsch,[66] C. D. Fu,[1] Y. W. Fu,[1] H. Gao,[61] Y. N. Gao,[45,g] Yang Gao,[69,56] S. Garbolino,[72c] I. Garzia,[29a,29b] P. T. Ge,[74] Z. W. Ge,[41] C. Geng,[57] E. M. Gersabeck,[65] A. Gilman,[67] K. Goetzen,[14] L. Gong,[39] W. X. Gong,[1,56] W. Gradl,[34] S. Gramigna,[29a,29b] M. Greco,[72a,72c] M. H. Gu,[1,56] Y. T. Gu,[16] C. Y. Guan,[1,61] Z. L. Guan,[22] A. Q. Guo,[30,61] L. B. Guo,[40] R. P. Guo,[47] Y. P. Guo,[12,f] A. Guskov,[35,a] X. T. H.,[1,61] W. Y. Han,[38] X. Q. Hao,[20] F. A. Harris,[63] K. K. He,[53] K. L. He,[1,61] F. H. Heinsius,[4] C. H. Heinz,[34] Y. K. Heng,[1,56,61] C. Herold,[58] T. Holtmann,[4] P. C. Hong,[12,f] G. Y. Hou,[1,61] Y. R. Hou,[61] Z. L. Hou,[1] H. M. Hu,[1,61] J. F. Hu,[54,i] T. Hu,[1,56,61] Y. Hu,[1] G. S. Huang,[69,56] K. X. Huang,[57] L. Q. Huang,[30,61] X. T. Huang,[48] Y. P. Huang,[1] T. Hussain,[71] N. Hüsken,[27,34] W. Imoehl,[27] M. Irshad,[69,56] J. Jackson,[27] S. Jaeger,[4] S. Janchiv,[31] J. H. Jeong,[10] Q. Ji,[1] Q. P. Ji,[20] X. B. Ji,[1,61] X. L. Ji,[1,56] Y. Y. Ji,[48] Z. K. Jia,[69,56] P. C. Jiang,[45,g] S. S. Jiang,[38] T. J. Jiang,[17] X. S. Jiang,[1,56,61] Y. Jiang,[61] J. B. Jiao,[48] Z. Jiao,[23] S. Jin,[41] Y. Jin,[64] M. Q. Jing,[1,61] T. Johansson,[73] X. K.,[1] S. Kabana,[32] N. Kalantar-Nayestanaki,[62] X. L. Kang,[9] X. S. Kang,[39] R. Kappert,[62] M. Kavatsyuk,[62] B. C. Ke,[79] A. Khoukaz,[66] R. Kiuchi,[1] R. Kliemt,[14] L. Koch,[36] O. B. Kolcu,[60a] B. Kopf,[4] M. Kuessner,[4] A. Kupsc,[43,73] W. Kühn,[36] J. J. Lane,[65] J. S. Lange,[36] P. Larin,[19] A. Lavania,[26] L. Lavezzi,[72a,72c] T. T. Lei,[69,k] Z. H. Lei,[69,56] H. Leithoff,[34] M. Lellmann,[34] T. Lenz,[34] C. Li,[42] C. Li,[46] C. H. Li,[38] Cheng Li,[69,56] D. M. Li,[79] F. Li,[1,56] G. Li,[1] H. Li,[69,56] H. B. Li,[1,61] H. J. Li,[20] H. N. Li,[54,i] Hui Li,[42] J. R. Li,[59] J. S. Li,[57] J. W. Li,[48] Ke Li,[1] L. J. Li,[1,61] L. K. Li,[1] Lei Li,[3] M. H. Li,[42] P. R. Li,[37,j,k] S. X. Li,[12] T. Li,[48] W. D. Li,[1,61] W. G. Li,[1] X. H. Li,[69,56] X. L. Li,[48] Xiaoyu Li,[1,61] Y. G. Li,[45,g] Z. J. Li,[57] Z. X. Li,[16] Z. Y. Li,[57] C. Liang,[41] H. Liang,[69,56] H. Liang,[1,61] H. Liang,[33] Y. F. Liang,[52] Y. T. Liang,[30,61] G. R. Liao,[15] L. Z. Liao,[48] J. Libby,[26] A. Limphirat,[58] D. X. Lin,[30,61] T. Lin,[1] B. J. Liu,[1] B. X. Liu,[74] C. Liu,[33] C. X. Liu,[1] D. Liu,[19,69] F. H. Liu,[51] Fang Liu,[1] Feng Liu,[6] G. M. Liu,[54,i] H. Liu,[37,j,k] H. B. Liu,[16] H. M. Liu,[1,61] Huanhuan Liu,[1] Huihui Liu,[21] J. B. Liu,[69,56] J. L. Liu,[70] J. Y. Liu,[1,61] K. Liu,[1] K. Y. Liu,[39] Ke Liu,[22] L. Liu,[69,56] L. C. Liu,[42] Lu Liu,[42] M. H. Liu,[12,f] P. L. Liu,[1] Q. Liu,[61] S. B. Liu,[69,56] T. Liu,[12,f] W. K. Liu,[42] W. M. Liu,[69,56] X. Liu,[37,j,k] Y. Liu,[37,j,k] Y. B. Liu,[42] Z. A. Liu,[1,56,61] Z. Q. Liu,[48] X. C. Lou,[1,56,61] F. X. Lu,[57] H. J. Lu,[23] J. G. Lu,[1,56] X. L. Lu,[1] Y. Lu,[7] Y. P. Lu,[1,56] Z. H. Lu,[1,61] C. L. Luo,[40] M. X. Luo,[78] T. Luo,[12,f] X. L. Luo,[1,56] X. R. Lyu,[61] Y. F. Lyu,[42] F. C. Ma,[39] H. L. Ma,[1] J. L. Ma,[1,61] L. L. Ma,[48] M. M. Ma,[1,61] Q. M. Ma,[1] R. Q. Ma,[1,61] R. T. Ma,[61] X. Y. Ma,[1,56] Y. Ma,[45,g] F. E. Maas,[19] M. Maggiora,[72a,72c] S. Maldaner,[4] S. Malde,[67] A. Mangoni,[28b] Y. J. Mao,[45,g] Z. P. Mao,[1] S. Marcello,[72a,72c] Z. X. Meng,[64] J. G. Messchendorp,[14,62] G. Mezzadri,[29a] H. Miao,[1,61] T. J. Min,[41] R. E. Mitchell,[27] X. H. Mo,[1,56,61] N. Yu. Muchnoi,[13,b] Y. Nefedov,[35] F. Nerling,[19,d] I. B. Nikolaev,[13,b] Z. Ning,[1,56] S. Nisar,[11,l] Y. Niu,[48] S. L. Olsen,[61] Q. Ouyang,[1,56,61] S. Pacetti,[28b,28c] X. Pan,[53] Y. Pan,[55] A. Pathak,[33] Y. P. Pei,[69,56] M. Pelizaeus,[4] H. P. Peng,[69,56] K. Peters,[14,d] J. L. Ping,[40] R. G. Ping,[1,61] S. Plura,[34] S. Pogodin,[35] V. Prasad,[32] F. Z. Qi,[1] H. Qi,[69,56] H. R. Qi,[59] M. Qi,[41] T. Y. Qi,[12,f] S. Qian,[1,56] W. B. Qian,[61] C. F. Qiao,[61] J. J. Qin,[70] L. Q. Qin,[15] X. P. Qin,[12,f] X. S. Qin,[48] Z. H. Qin,[1,56] J. F. Qiu,[1] S. Q. Qu,[59] C. F. Redmer,[34] K. J. Ren,[38] A. Rivetti,[72c] V. Rodin,[62] M. Rolo,[72c] G. Rong,[1,61] Ch. Rosner,[19] S. N. Ruan,[42] N. Salone,[43] A. Sarantsev,[35,c] Y. Schelhaas,[34] K. Schoenning,[73] M. Scodeggio,[29a,29b] K. Y. Shan,[12,f] W. Shan,[24] X. Y. Shan,[69,56] J. F. Shangguan,[53] L. G. Shao,[1,61] M. Shao,[69,56] C. P. Shen,[12,f] H. F. Shen,[1,61] W. H. Shen,[61] X. Y. Shen,[1,61] B. A. Shi,[61] H. C. Shi,[69,56] J. L. Shi,[12] J. Y. Shi,[1] Q. Q. Shi,[53] R. S. Shi,[1,61] X. Shi,[1,56] J. J. Song,[20] T. Z. Song,[57] W. M. Song,[33,1] Y. J. Song,[12] Y. X. Song,[45,g] S. Sosio,[72a,72c] S. Spataro,[72a,72c] F. Stieler,[34] Y. J. Su,[61] G. B. Sun,[74] G. X. Sun,[1] H. Sun,[61] H. K. Sun,[1] J. F. Sun,[20] K. Sun,[59] L. Sun,[74] S. S. Sun,[1,61] T. Sun,[1,61] W. Y. Sun,[33] Y. Sun,[9] Y. J. Sun,[69,56] Y. Z. Sun,[1] Z. T. Sun,[48] Y. X. Tan,[69,56] C. J. Tang,[52] G. Y. Tang,[1] J. Tang,[57] Y. A. Tang,[74] L. Y. Tao,[70] Q. T. Tao,[25,h] M. Tat,[67] J. X. Teng,[69,56] V. Thoren,[73] W. H. Tian,[57] W. H. Tian,[50] Y. Tian,[30,61] Z. F. Tian,[74] I. Uman,[60b] B. Wang,[1] B. L. Wang,[61] Bo Wang,[69,56] C. W. Wang,[41] D. Y. Wang,[45,g] F. Wang,[70]

H. J. Wang,[37,j,k] H. P. Wang,[1,61] K. Wang,[1,56] L. L. Wang,[1] M. Wang,[48] Meng Wang,[1,61] S. Wang,[12,f] S. Wang,[37,j,k] T. Wang,[12,f] T. J. Wang,[42] W. Wang,[70] W. Wang,[57] W. H. Wang,[74] W. P. Wang,[69,56] X. Wang,[45,g] X. F. Wang,[37,j,k] X. J. Wang,[38] X. L. Wang,[12,f] Y. Wang,[59] Y. D. Wang,[44] Y. F. Wang,[1,56,61] Y. H. Wang,[46] Y. N. Wang,[44] Y. Q. Wang,[1] Yaqian Wang,[18,1] Yi Wang,[59] Z. Wang,[1,56] Z. L. Wang,[70] Z. Y. Wang,[1,61] Ziyi Wang,[61] D. Wei,[68] D. H. Wei,[15] F. Weidner,[66] S. P. Wen,[1] C. W. Wenzel,[4] U. Wiedner,[4] G. Wilkinson,[67] M. Wolke,[73] L. Wollenberg,[4] C. Wu,[38] J. F. Wu,[1,61] L. H. Wu,[1] L. J. Wu,[1,61] X. Wu,[12,f] X. H. Wu,[33] Y. Wu,[69] Y. J. Wu,[30] Z. Wu,[1,56] L. Xia,[69,56] X. M. Xian,[38] T. Xiang,[45,g] D. Xiao,[37,j,k] G. Y. Xiao,[41] H. Xiao,[12,f] S. Y. Xiao,[1] Y. L. Xiao,[12,f] Z. J. Xiao,[40] C. Xie,[41] X. H. Xie,[45,g] Y. Xie,[48] Y. G. Xie,[1,56] Y. H. Xie,[6] Z. P. Xie,[69,56] T. Y. Xing,[1,61] C. F. Xu,[1,61] C. J. Xu,[57] G. F. Xu,[1] H. Y. Xu,[64] Q. J. Xu,[17] W. L. Xu,[64] X. P. Xu,[53] Y. C. Xu,[76] Z. P. Xu,[41] F. Yan,[12,f] L. Yan,[12,f] W. B. Yan,[69,56] W. C. Yan,[79] X. Q. Yan,[1] H. J. Yang,[49,e] H. L. Yang,[33] H. X. Yang,[1] Tao Yang,[1] Y. Yang,[12,f] Y. F. Yang,[42] Y. X. Yang,[1,61] Yifan Yang,[1,61] Z. W. Yang,[37,j,k] M. Ye,[1,56] M. H. Ye,[8] J. H. Yin,[1] Z. Y. You,[57] B. X. Yu,[1,56,61] C. X. Yu,[42] G. Yu,[1,61] T. Yu,[70] X. D. Yu,[45,g] C. Z. Yuan,[1,61] L. Yuan,[2] S. C. Yuan,[1] X. Q. Yuan,[1] Y. Yuan,[1,61] Z. Y. Yuan,[57] C. X. Yue,[38] A. A. Zafar,[71] F. R. Zeng,[48] X. Zeng,[12,f] Y. Zeng,[25,h] Y. J. Zeng,[1,61] X. Y. Zhai,[33] Y. H. Zhan,[57] A. Q. Zhang,[1,61] B. L. Zhang,[1,61] B. X. Zhang,[1] D. H. Zhang,[42] G. Y. Zhang,[20] H. Zhang,[69] H. H. Zhang,[57] H. H. Zhang,[33] H. Q. Zhang,[1,56,61] H. Y. Zhang,[1,56] J. J. Zhang,[50] J. L. Zhang,[75] J. Q. Zhang,[40] J. W. Zhang,[1,56,61] J. X. Zhang,[37,j,k] J. Y. Zhang,[1] J. Z. Zhang,[1,61] Jiawei Zhang,[1,61] L. M. Zhang,[59] L. Q. Zhang,[57] Lei Zhang,[41] P. Zhang,[1] Q. Y. Zhang,[38,79] Shuihan Zhang,[1,61] Shulei Zhang,[25,h] X. D. Zhang,[44] X. M. Zhang,[1] X. Y. Zhang,[53] X. Y. Zhang,[48] Y. Zhang,[67] Y. T. Zhang,[79] Y. H. Zhang,[1,56] Yan Zhang,[69,56] Yao Zhang,[1] Z. H. Zhang,[1] Z. L. Zhang,[33] Z. Y. Zhang,[74] Z. Y. Zhang,[42] G. Zhao,[1] J. Zhao,[38] J. Y. Zhao,[1,61] J. Z. Zhao,[1,56] Lei Zhao,[69,56] Ling Zhao,[1] M. G. Zhao,[42] S. J. Zhao,[79] Y. B. Zhao,[1,56] Y. X. Zhao,[30,61] Z. G. Zhao,[69,56] A. Zhemchugov,[35,a] B. Zheng,[70] J. P. Zheng,[1,56] W. J. Zheng,[1,61] Y. H. Zheng,[61] B. Zhong,[40] X. Zhong,[57] H. Zhou,[48] L. P. Zhou,[1,61] X. Zhou,[74] X. K. Zhou,[6] X. R. Zhou,[69,56] X. Y. Zhou,[38] Y. Z. Zhou,[12,f] J. Zhu,[42] K. Zhu,[1] K. J. Zhu,[1,56,61] L. Zhu,[33] L. X. Zhu,[61] S. H. Zhu,[68] S. Q. Zhu,[41] T. J. Zhu,[12,f] W. J. Zhu,[12,f] Y. C. Zhu,[69,56] Z. A. Zhu,[1,61] J. H. Zou,[1] and J. Zu[69,56]

(BESIII Collaboration)

[1]*Institute of High Energy Physics, Beijing 100049, People's Republic of China*
[2]*Beihang University, Beijing 100191, People's Republic of China*
[3]*Beijing Institute of Petrochemical Technology, Beijing 102617, People's Republic of China*
[4]*Bochum Ruhr-University, D-44780 Bochum, Germany*
[5]*Carnegie Mellon University, Pittsburgh, Pennsylvania 15213, USA*
[6]*Central China Normal University, Wuhan 430079, People's Republic of China*
[7]*Central South University, Changsha 410083, People's Republic of China*
[8]*China Center of Advanced Science and Technology, Beijing 100190, People's Republic of China*
[9]*China University of Geosciences, Wuhan 430074, People's Republic of China*
[10]*Chung-Ang University, Seoul 06974, Republic of Korea*
[11]*COMSATS University Islamabad, Lahore Campus,*
Defence Road, Off Raiwind Road, 54000 Lahore, Pakistan
[12]*Fudan University, Shanghai 200433, People's Republic of China*
[13]*G.I. Budker Institute of Nuclear Physics SB RAS (BINP), Novosibirsk 630090, Russia*
[14]*GSI Helmholtzcentre for Heavy Ion Research GmbH, D-64291 Darmstadt, Germany*
[15]*Guangxi Normal University, Guilin 541004, People's Republic of China*
[16]*Guangxi University, Nanning 530004, People's Republic of China*
[17]*Hangzhou Normal University, Hangzhou 310036, People's Republic of China*
[18]*Hebei University, Baoding 071002, People's Republic of China*
[19]*Helmholtz Institute Mainz, Staudinger Weg 18, D-55099 Mainz, Germany*
[20]*Henan Normal University, Xinxiang 453007, People's Republic of China*
[21]*Henan University of Science and Technology, Luoyang 471003, People's Republic of China*
[22]*Henan University of Technology, Zhengzhou 450001, People's Republic of China*
[23]*Huangshan College, Huangshan 245000, People's Republic of China*
[24]*Hunan Normal University, Changsha 410081, People's Republic of China*
[25]*Hunan University, Changsha 410082, People's Republic of China*
[26]*Indian Institute of Technology Madras, Chennai 600036, India*
[27]*Indiana University, Bloomington, Indiana 47405, USA*
[28a]*INFN Laboratori Nazionali di Frascati, Italy*

[28b]INFN Sezione di Perugia, I-06100, Perugia, Italy

[28c]University of Perugia, I-06100, Perugia, Italy

[29a]INFN Sezione di Ferrara, I-44122, Ferrara, Italy

[29b]University of Ferrara, I-44122, Ferrara, Italy

[30]Institute of Modern Physics, Lanzhou 730000, People's Republic of China

[31]Institute of Physics and Technology, Peace Avenue 54B, Ulaanbaatar 13330, Mongolia

[32]Instituto de Alta Investigación, Universidad de Tarapacá, Casilla 7D, Arica, Chile

[33]Jilin University, Changchun 130012, People's Republic of China

[34]Johannes Gutenberg University of Mainz, Johann-Joachim-Becher-Weg 45, D-55099 Mainz, Germany

[35]Joint Institute for Nuclear Research, 141980 Dubna, Moscow region, Russia

[36]Justus-Liebig-Universitaet Giessen, II. Physikalisches Institut,
Heinrich-Buff-Ring 16, D-35392 Giessen, Germany

[37]Lanzhou University, Lanzhou 730000, People's Republic of China

[38]Liaoning Normal University, Dalian 116029, People's Republic of China

[39]Liaoning University, Shenyang 110036, People's Republic of China

[40]Nanjing Normal University, Nanjing 210023, People's Republic of China

[41]Nanjing University, Nanjing 210093, People's Republic of China

[42]Nankai University, Tianjin 300071, People's Republic of China

[43]National Centre for Nuclear Research, Warsaw 02-093, Poland

[44]North China Electric Power University, Beijing 102206, People's Republic of China

[45]Peking University, Beijing 100871, People's Republic of China

[46]Qufu Normal University, Qufu 273165, People's Republic of China

[47]Shandong Normal University, Jinan 250014, People's Republic of China

[48]Shandong University, Jinan 250100, People's Republic of China

[49]Shanghai Jiao Tong University, Shanghai 200240, People's Republic of China

[50]Shanxi Normal University, Linfen 041004, People's Republic of China

[51]Shanxi University, Taiyuan 030006, People's Republic of China

[52]Sichuan University, Chengdu 610064, People's Republic of China

[53]Soochow University, Suzhou 215006, People's Republic of China

[54]South China Normal University, Guangzhou 510006, People's Republic of China

[55]Southeast University, Nanjing 211100, People's Republic of China

[56]State Key Laboratory of Particle Detection and Electronics,
Beijing 100049, Hefei 230026, People's Republic of China

[57]Sun Yat-Sen University, Guangzhou 510275, People's Republic of China

[58]Suranaree University of Technology, University Avenue 111, Nakhon Ratchasima 30000, Thailand

[59]Tsinghua University, Beijing 100084, People's Republic of China

[60a]Turkish Accelerator Center Particle Factory Group, Istinye University, 34010, Istanbul, Turkey

[60b]Near East University, Nicosia, North Cyprus, 99138, Mersin 10, Turkey

[61]University of Chinese Academy of Sciences, Beijing 100049, People's Republic of China

[62]University of Groningen, NL-9747 AA Groningen, Netherlands

[63]University of Hawaii, Honolulu, Hawaii 96822, USA

[64]University of Jinan, Jinan 250022, People's Republic of China

[65]University of Manchester, Oxford Road, Manchester, M13 9PL, United Kingdom

[66]University of Muenster, Wilhelm-Klemm-Strasse 9, 48149 Muenster, Germany

[67]University of Oxford, Keble Road, Oxford OX13RH, United Kingdom

[68]University of Science and Technology Liaoning, Anshan 114051, People's Republic of China

[69]University of Science and Technology of China, Hefei 230026, People's Republic of China

[70]University of South China, Hengyang 421001, People's Republic of China

[71]University of the Punjab, Lahore-54590, Pakistan

[72a]University of Turin and INFN, University of Turin, I-10125, Turin, Italy

[72b]University of Eastern Piedmont, I-15121, Alessandria, Italy

[72c]INFN, I-10125, Turin, Italy

[73]Uppsala University, Box 516, SE-75120 Uppsala, Sweden

[74]Wuhan University, Wuhan 430072, People's Republic of China

[75]Xinyang Normal University, Xinyang 464000, People's Republic of China

[76]Yantai University, Yantai 264005, People's Republic of China

[77]Yunnan University, Kunming 650500, People's Republic of China

[78]*Zhejiang University, Hangzhou 310027, People's Republic of China*
[79]*Zhengzhou University, Zhengzhou 450001, People's Republic of China*

A precision measurement of the matrix elements for $\eta \to \pi^+\pi^-\pi^0$ and $\eta \to \pi^0\pi^0\pi^0$ decays is performed using a sample of $(10087 \pm 44) \times 10^6$ J/ψ decays collected with the BESIII detector. The decay $J/\psi \to \gamma\eta$ is used to select clean samples of $631,686$ $\eta \to \pi^+\pi^-\pi^0$ decays and $272,322$ $\eta \to \pi^0\pi^0\pi^0$ decays. The matrix elements for both channels are in reasonable agreement with previous measurements. The nonzero gX^2Y term for the decay mode $\eta \to \pi^+\pi^-\pi^0$ is confirmed, as reported by the KLOE Collaboration, while the other higher-order terms are found to be insignificant. Dalitz plot asymmetries in the $\eta \to \pi^+\pi^-\pi^0$ decay are also explored and are found to be consistent with charge conjugation invariance. In addition, a cusp effect is investigated in the $\eta \to \pi^0\pi^0\pi^0$ decay, and no obvious structure around the $\pi^+\pi^-$ mass threshold is observed.

I. INTRODUCTION

The decay of the η meson into 3π violates isospin symmetry and is related to the difference of light-quark masses, $m_u - m_d$, where m_u and m_d are the masses of valence quark u and d, respectively. Therefore, the decay $\eta \to 3\pi$ offers a unique way to determine the quark mass

[a]Also at the Moscow Institute of Physics and Technology, Moscow 141700, Russia.
[b]Also at the Novosibirsk State University, Novosibirsk 630090, Russia.
[c]Also at the NRC "Kurchatov Institute", PNPI, 188300 Gatchina, Russia.
[d]Also at Goethe University Frankfurt, 60323 Frankfurt am Main, Germany.
[e]Also at Key Laboratory for Particle Physics, Astrophysics and Cosmology, Ministry of Education; Shanghai Key Laboratory for Particle Physics and Cosmology; Institute of Nuclear and Particle Physics, Shanghai 200240, People's Republic of China.
[f]Also at Key Laboratory of Nuclear Physics and Ion-beam Application (MOE) and Institute of Modern Physics, Fudan University, Shanghai 200443, People's Republic of China.
[g]Also at State Key Laboratory of Nuclear Physics and Technology, Peking University, Beijing 100871, People's Republic of China.
[h]Also at School of Physics and Electronics, Hunan University, Changsha 410082, China.
[i]Also at Guangdong Provincial Key Laboratory of Nuclear Science, Institute of Quantum Matter, South China Normal University, Guangzhou 510006, China.
[j]Also at Frontiers Science Center for Rare Isotopes, Lanzhou University, Lanzhou 730000, China.
[k]Also at Lanzhou Center for Theoretical Physics, Lanzhou University, Lanzhou 730000, China.
[l]Also at the Department of Mathematical Sciences, IBA, Karachi, Pakistan.

ratio $Q^2 \equiv (m_s^2 - \hat{m}^2)/(m_d^2 - m_u^2)$, where $\hat{m} = \frac{1}{2}(m_d + m_u)$. This has stimulated both theoretical and experimental interest [1]. Extensive theoretical studies have been performed within the framework of combined chiral perturbation theory (ChPT) and dispersion theory [2–7]. Experimentally, the most recent results are from the WASA-at-COSY [8,9], KLOE/KLOE-2 [10,11], BESIII [12] (with 1.3 billion J/ψ events collected in 2009 and 2012), and A2 [13] Collaborations. Taking experimental results as inputs, two dedicated analyses by independent groups of theorists reported $Q = 22.0 \pm 0.7$ [14] and $Q = 21.6 \pm 1.1$ [15].

In addition, a sizeable cusp structure is expected to be visible in the mass spectra of $\pi^0\pi^0$ for $\eta \to \pi^0\pi^0\pi^0$ around the $\pi^+\pi^-$ mass threshold [16,17], corresponding to the virtual transition $\pi^0\pi^0 \to \pi^+\pi^- \to \pi^0\pi^0$ [7]. An analogous cusp was first predicted [18] and then observed in the $K^+ \to \pi^+\pi^0\pi^0$ by the NA48/2 Collaboration [19]. Furthermore, the BESIII collaboration observed the evidence of a cusp structure with a statistical significance of around 3.5σ in $\eta' \to \eta\pi^0\pi^0$ [20], which is consistent with the cusp effect predicted by the nonrelativistic effective field theory (NREFT) [21]. A series of experimental efforts have been spent to investigate the Dalitz plot of $\eta \to \pi^0\pi^0\pi^0$ decays [9,11,12], but no obvious cusp effect has yet been observed. The most recent result from the A2 Collaboration [13] stated that it is necessary to introduce the cusp effect term in order to better describe their experimental data, but the effect included a large uncertainty of about 50%.

With the additional J/ψ data collected in 2018 and 2019, the total number of J/ψ decays accumulated with the BESIII detector has increased to $(10087 \pm 44) \times 10^6$ [22], which is about 8 times larger than the sample used in the previous BESIII analysis [12]. This provides a unique opportunity to further investigate the decays $\eta \to \pi^+\pi^-\pi^0$ and $\eta \to \pi^0\pi^0\pi^0$. In this paper, the parametrizations of the Dalitz plot amplitudes for $\eta \to \pi^+\pi^-\pi^0$ and $\eta \to \pi^0\pi^0\pi^0$

decays follow the previous measurements and are briefly described below.

The Dalitz plot for the mode $\eta \to \pi^+\pi^-\pi^0$ is generally described by the following two variables [12]

$$X = \frac{\sqrt{3}}{Q_\eta}(T_{\pi^+} - T_{\pi^-}), \qquad Y = \frac{3T_{\pi^0}}{Q_\eta} - 1, \qquad (1)$$

where T_π denotes the kinetic energy of a given pion in the η rest frame, $Q_\eta = m_\eta - m_{\pi^+} - m_{\pi^-} - m_{\pi^0}$ is the excess energy of the reaction, and $m_{\eta/\pi}$ are the nominal masses from the Particle Data Group (PDG) [23]. The square of the decay amplitude can be parametrized as

$$|A(X, Y)|^2 \propto 1 + aY + bY^2 + cX + dX^2 + eXY$$
$$+ fY^3 + gX^2Y + \cdots, \qquad (2)$$

where the parameters a, b, c, d, … are the matrix elements used to test theoretical predictions and fundamental symmetries. Specifically, nonzero odd terms of X (c and e) and integrated asymmetries [24] in the Dalitz plot imply the violation of charge conjugation symmetry.

For the decay $\eta \to \pi^0\pi^0\pi^0$, the density distribution of the Dalitz plot has threefold symmetry due to the three identical π^0s in the final state. Hence, the density distribution can be parametrized using a polar variable

$$Z = X^2 + Y^2 = \frac{2}{3}\sum_{i=1}^{3}\left(\frac{3T_i}{Q_\eta} - 1\right)^2, \qquad (3)$$

and the square of the decay amplitude is expanded as [4,5]

$$|A(X, Y)|^2 \propto 1 + 2\alpha Z + 2\beta(3X^2Y - Y^3) + 2\gamma Z^2 + \cdots, \qquad (4)$$

where α, β, and γ are the slope parameters, $Q_\eta = m_\eta - 3m_{\pi^0}$, and T_i denotes the kinetic energy of each π^0 in the η rest frame. Due to the low energies of the final state particles, the $\pi^0\pi^0$ rescattering in $\eta \to \pi^0\pi^0\pi^0$ is expected to be dominated by the S-wave, which leads to the conventional amplitude parametrization $|A(Z)|^2 \propto 1 + 2\alpha Z$ of $\eta \to \pi^0\pi^0\pi^0$, and is widely used in most of the previous measurements [10,12,25]. However, the existence of the cusp effect allows nonzero contributions from higher order terms, as was first explored by the A2 Collaboration [13].

II. DETECTOR AND MONTE CARLO SIMULATION

The BESIII detector [26] records symmetric e^+e^- collisions provided by the BEPCII storage rings [27], which operate in the center-of-mass energy range from 2.00 to 4.95 GeV, with a peak luminosity of 1×10^{33} cm^{-2} s^{-1} achieved at $\sqrt{s} = 3.77$ GeV. The BESIII detector has

collected large data samples in this energy region [28]. The cylindrical core of the BESIII detector covers 93% of the full solid angle and consists of a helium-based multilayer drift chamber (MDC), a plastic scintillator time-of-flight system (TOF), and a CsI(TI) electromagnetic calorimeter (EMC), which are all enclosed in a superconducting solenoidal magnet providing a 1.0 T (0.9 T in 2012) magnetic field [29]. The solenoid is supported by an octagonal flux-return yoke with resistive plate counter muon identification modules interleaved with steel. The charged-particle momentum resolution at 1 GeV/c is 0.5%, and the specific ionization energy loss dE/dx resolution is 6% for electrons from the Bhabha scattering. The EMC measures cluster energies with a resolution of 2.5% (5%) at 1 GeV in the barrel (end cap) region. The time resolution in the TOF barrel region is 68 ps, while that in the end cap region is 110 ps. The end cap TOF system was upgraded in 2015 using multigap resistive plate chamber technology, providing a time resolution of 60 ps [30,31].

Simulated data samples produced with a GEANT4-based [32] Monte Carlo (MC) package, which includes the geometric description of the BESIII detector and the detector response, are used to determine detection efficiencies and to estimate backgrounds. The simulation models the beam energy spread and initial state radiation in the e^+e^- annihilation with the generator KKMC [33,34]. A simulated sample of 10 billion J/ψ inclusive decays (inclusive MC sample) including both the production of the J/ψ resonance and the continuum processes is produced with KKMC to identify background contributions. All particle decays are modelled with EVTGEN [35,36] using branching fractions either taken from the PDG [23], when available, or otherwise estimated with LUNDCHARM [37,38]. Final state radiation from charged final state particles is incorporated using the PHOTOS package [39].

III. ANALYSIS OF THE DECAY $\eta \to \pi^+\pi^-\pi^0$

To reconstruct $J/\psi \to \gamma\eta$ with the subsequent decays $\eta \to \pi^+\pi^-\pi^0$ and $\pi^0 \to \gamma\gamma$, candidate events are required to have exactly two oppositely charged tracks and at least three photon candidates. Charged tracks detected in the MDC are required to be within a polar angle (θ) range of $|\cos\theta| < 0.93$, where θ is defined with respect to the z-axis, which is the symmetry axis of the MDC. The distance of closest approach for each track must be less than 10 cm along the positron beam direction and less than 1 cm in the transverse plane with respect to the interaction point (IP). Photon candidates, identified using isolated clusters in the EMC, are required to have a deposited energy greater than 25 MeV in the barrel region ($|\cos\theta| < 0.80$) and 50 MeV in the endcap region ($0.86 < |\cos\theta| < 0.92$). To eliminate clusters originating from charged tracks, the angle subtended by the EMC cluster and the position of the closest charged track at the EMC must be greater than 10 degrees as measured from the IP. The difference
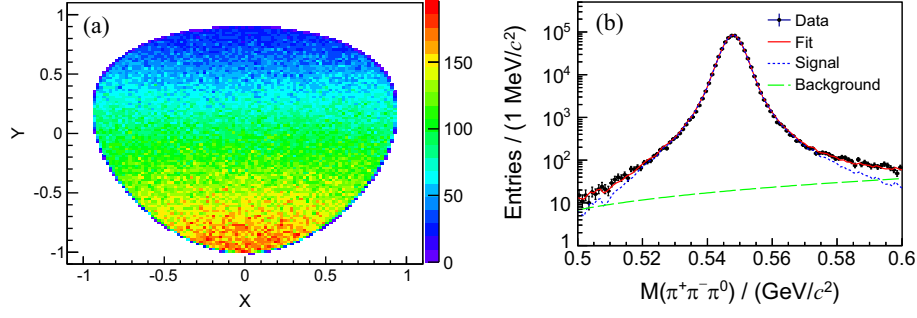
FIG. 1. (a) Dalitz plot for $\eta \to \pi^+\pi^-\pi^0$ candidate events selected from data. (b) Invariant mass distribution of $\pi^+\pi^-\pi^0$ candidates without the η mass constraint applied in the kinematic fit.

between the EMC time and the event start time is required to be within [0, 700] ns to suppress electronic noise and energy deposition unrelated to the event.

Since the radiative photon from the J/ψ decay is always more energetic than the photons from the π^0 decay, the photon candidate with the maximum energy in the event is taken as the radiative one. For each $\pi^+\pi^-\gamma\gamma$ combination, a six-constraint (6C) kinematic fit is performed, and the χ^2_{6C} is required to be less than 80. The fit enforces energy-momentum conservation (4C) and constrains the invariant masses of the other two photons and $\pi^+\pi^-\pi^0$ to the nominal π^0 and η masses, respectively. If there are more than three photon candidates in an event, the combination with the smallest χ^2_{6C} is retained. Possible background events are investigated with an inclusive MC sample of 10 billion J/ψ events. To reject background events with two or four photons in the final state, we further require that the probability of the 4C kinematic fit imposing energy-momentum conservation for the $J/\psi \to \pi^+\pi^-\gamma\gamma\gamma$ signal hypothesis is smaller than those for the $J/\psi \to \pi^+\pi^-\gamma\gamma$ and $J/\psi \to \pi^+\pi^-\gamma\gamma\gamma\gamma$ background hypotheses. After applying the above selection criteria, there are no peaking backgrounds in the η signal region and the background contamination ratio is estimated to be 0.12%. A sample of $631,686$ $\eta \to \pi^+\pi^-\pi^0$ candidate events is selected and the corresponding Dalitz plot of X versus Y is shown in Fig. 1(a). The overall efficiency is estimated to be $(25.57 \pm 0.01)\%$ using a dedicated MC simulation based on the previous BESIII measurement [12].

To estimate the background contribution under the η peak, a 5C kinematic fit without the η mass constraint is performed. The resulting $\pi^+\pi^-\pi^0$ invariant mass spectrum, $M(\pi^+\pi^-\pi^0)$, is shown in Fig. 1(b), where a clear η peak is observed. An unbinned maximum likelihood fit is then performed to the $M(\pi^+\pi^-\pi^0)$ distribution, where the signal is described by the MC-simulated shape convolved with a Gaussian resolution function, and the background contribution is described by a second-order Chebyshev polynomial function. The background fraction is estimated to be about 0.10% in the η signal region $(0.528, 0.568)$ GeV/c^2, which is consistent with the estimation from the inclusive

MC sample. Therefore, the background contribution is neglected in the extraction of the matrix elements.

An unbinned maximum likelihood fit to data is performed to extract the free parameters in the decay amplitude given in Eq. (2). To account for the resolution and detection efficiency, the amplitude squared is convolved with a function $\sigma(X, Y)$ parametrizing the resolution and multiplied by a function $\varepsilon(X, Y)$ representing the detection efficiency. Both functions are derived from the dedicated MC simulation based on the previous BESIII measurement [12]. Two double Gaussian functions are used for $\sigma(X, Y)$, while $\varepsilon(X, Y)$ is estimated as the average efficiency within a given bin of X and Y. The probability density function $\mathcal{P}(X, Y)$ applied to data is defined as

$$\mathcal{P}(X, Y) = \frac{(|A(X, Y)|^2 \otimes \sigma(X, Y)) \cdot \varepsilon(X, Y)}{\int_{DP}((|A(X, Y)|^2 \otimes \sigma(X, Y)) \cdot \varepsilon(X, Y))dXdY}.$$

(5)

The integral over the full Dalitz plot range (DP) gives the normalization factor in the denominator. The fit is done by minimizing the negative log-likelihood value

$$-\ln \mathcal{L} = -\sum_{i=1}^{N_{\text{event}}} \ln \mathcal{P}(X_i, Y_i),$$

(6)

where $\mathcal{P}(X_i, Y_i)$ is evaluated for the event i, and the sum runs over all accepted events.

Ignoring the high-order term gX^2Y and imposing charge conjugation invariance by setting the coefficient of odd powers in X (c and e) to zero, the fit yields the following parameters

$$a = -1.097 \pm 0.005,$$
$$b = 0.158 \pm 0.006,$$
$$d = 0.070 \pm 0.006,$$
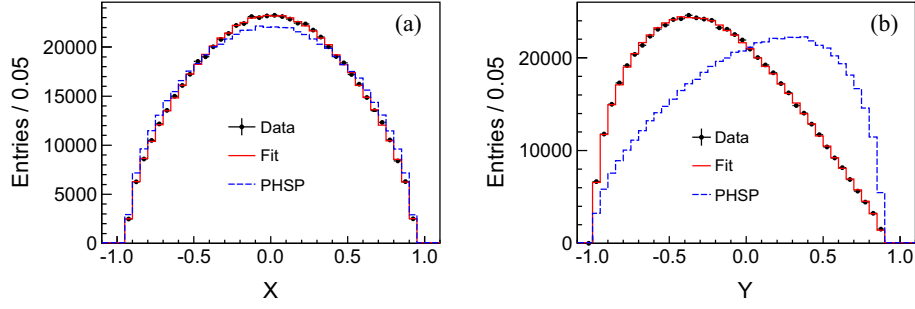$$f = 0.134 \pm 0.010,$$

(7)

and the corresponding correlation matrix

FIG. 2.   Projections of the Dalitz plot on (a) X and (b) Y for $\eta \to \pi^+\pi^-\pi^0$ candidates, where the dots with error bars are data, the dashed histograms are PHSP-distributed MC events, and the solid histograms are the fit projections.

$$
\begin{pmatrix}
 & a & b & d & f \\
\hline
a & 1.000 & -0.262 & -0.384 & -0.751 \\
b & & 1.000 & 0.310 & -0.294 \\
d & & & 1.000 & 0.076 \\
f & & & & 1.000
\end{pmatrix}. \quad (8)
$$

$$
\begin{pmatrix}
 & a & b & d & f & g \\
\hline
a & 1.000 & -0.124 & 0.005 & -0.785 & -0.470 \\
b & & 1.000 & 0.369 & -0.343 & -0.216 \\
d & & & 1.000 & -0.145 & -0.595 \\
f & & & & 1.000 & 0.344 \\
g & & & & & 1.000
\end{pmatrix}.
$$

$$(10)$$

Here the uncertainties are statistical only. The fit projections on X and Y are illustrated as the solid histograms in Fig. 2(a) and Fig. 2(b). The obtained parameters are compatible with the previous BESIII measurement [12] but the statistical uncertainties are improved significantly. For comparison, the corresponding distributions obtained from phase space (PHSP) distributed MC simulated events of $\eta \to \pi^+\pi^-\pi^0$ are also shown in Fig. 2.

An alternative fit with parameters c and e free is also performed to search for the violation of charge conjugation symmetry. The fit yields $c = (-0.086 \pm 2.986) \times 10^{-3}$ and $e = -0.001 \pm 0.007$ which are consistent with zero within statistical uncertainties, while the derived parameters a, b, d, and f are almost unchanged. The statistical significance of charge-parity violation, determined by the changes of the log-likelihood value and the number of degrees of freedom, is calculated to be 0.7σ, which indicates that there is no evidence for charge-parity violation in the decay $\eta \to \pi^+\pi^-\pi^0$.

Another fit with the cubic term gX^2Y included is also performed. The fitted parameters and corresponding correlation matrix are

$$a = -1.086 \pm 0.006,$$
$$b = 0.162 \pm 0.006,$$
$$d = 0.083 \pm 0.007,$$
$$f = 0.118 \pm 0.011,$$
$$g = -0.053 \pm 0.017, \quad (9)$$

and

An evident contribution from the X^2Y term is found. Based on the change in the log-likelihood value and taking into account the change in the number of degrees of freedom, the statistical significance of a nonzero g is calculated to be 3.0σ. The value of g is in agreement with the first and only existing experimental measurement from the KLOE-2 Collaboration, $-0.044 \pm 0.009^{+0.012}_{-0.013}$ [11].

The impact of the extra charge conjugation symmetry violation terms $hXY^2 + lX^3$ are also investigated and the corresponding parameters are found to be $h = -0.006 \pm 0.010$ and $l = -0.0009 \pm 0.0060$, while the other parameters are unchanged, which means the contributions from these terms are not significant based on the current statistics.

In addition to terms with an odd power of X in Eq. (2), the unbinned integrated asymmetries of the Dalitz plot provide a more sensitive test of charge conjugation violation [11,24,40–45]. The left-right asymmetry (A_{LR}) can be used to check charge conjugation violation, the quadrant asymmetry (A_Q) is sensitive to charge conjugation violation when isospin changes by two units, $\Delta I = 2$, and the sextant asymmetry (A_S) is sensitive when $\Delta I = 0$. Following the same definitions as those used in the previous measurements [11,42] and using the detection efficiency corrected candidate events, the A_{LR}, A_Q, and A_Q are calculated to be

$$A_{LR} = (0.114 \pm 0.131)\%,$$
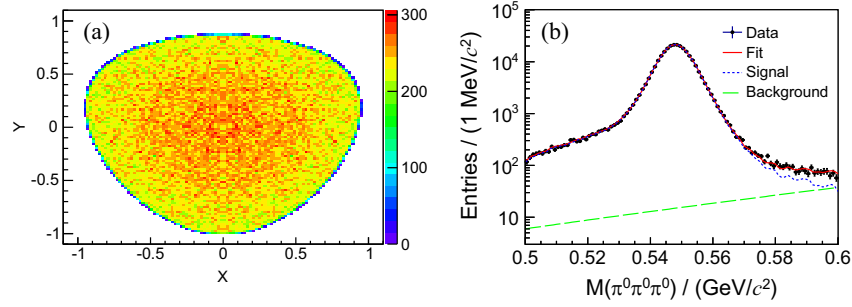$$A_Q = (-0.035 \pm 0.131)\%,$$
$$A_S = (-0.070 \pm 0.131)\%, \quad (11)$$

FIG. 3. (a) Dalitz plot for $\eta \to \pi^0\pi^0\pi^0$ candidate events selected from data (six entries per event). (b) Invariant mass spectrum of $\pi^0\pi^0\pi^0$ candidates without the η mass constraint applied in the kinematic fit.

where the uncertainties are statistical only, thereby indicating no evidence of deviation from zero.

IV. ANALYSIS OF THE DECAY $\eta \to \pi^0\pi^0\pi^0$

To reconstruct $J/\psi \to \gamma\eta$ with $\eta \to \pi^0\pi^0\pi^0$ and $\pi^0 \to \gamma\gamma$ candidate events, at least seven photons and no charged tracks are required. The selection criteria for the photon candidates are the same as those described above for $\eta \to \pi^+\pi^-\pi^0$, but no requirement on the angle between photon candidates and charged tracks is imposed. To suppress electronic noise and clusters unrelated to the event, the difference between the EMC time and the most energetic photon is required to be within $[-500, 500]$ ns. The photon with maximum energy in the event is assumed to be the radiative photon originating from the J/ψ decay. For the remaining photon candidates, all possible $\gamma\gamma$ pairs are combined into π^0 candidates and subjected separately to a one-constraint kinematic fit in which the invariant mass of the $\gamma\gamma$ is constrained to the nominal π^0 mass. The $\chi^2_{\pi^0}$ value of this kinematic fit is required to be less than 25. To suppress photon miscombinations, the polar angle of the π^0 decay in the π^0 helicity frame, defined as $|\cos\theta_{\text{decay}}| = |E_{\gamma 1} - E_{\gamma 2}|/p_{\pi^0}$, where $E_{\gamma 1}$, $E_{\gamma 2}$, and p_{π^0} are the photon energies and the π^0 momentum in the lab frame, respectively, is required to satisfy $|\cos\theta_{\text{decay}}| < 0.95$. Events with at least three accepted π^0 candidates are retained for further analysis.

An eight-constraint (8C) kinematic fit is performed and the resulting χ^2_{8C} is required to be less than 70. The 8C kinematic fit enforces energy-momentum conservation and constrains the invariant masses of the three $\gamma\gamma$ pairs and the $\pi^0\pi^0\pi^0$ to the nominal π^0 and η masses, respectively. If there is more than one combination in an event, the one with the smallest χ^2_{8C} is retained. After all selection criteria are imposed, 272, 322 $\eta \to \pi^0\pi^0\pi^0$ events are selected for further analysis and the corresponding Dalitz plot of X versus Y is shown in Fig. 3(a). The overall efficiency is estimated to be $(8.15 \pm 0.01)\%$ from the dedicated MC simulation based on the BESIII previous measurement [12]. As mentioned above, there are three identical π^0 in the

final state, so the variables X and Y can be determined in six different ways but with the same value for the variable Z. Therefore, one event contributes to six entries in Fig. 3(a). The distribution of the kinematic variable Z for the selected candidate events in data is shown in Fig. 4.

To estimate the background contribution under the η peak, a 7C kinematic fit without the η mass constraint is performed. The resulting $\pi^0\pi^0\pi^0$ invariant mass spectrum, $M(\pi^0\pi^0\pi^0)$, is shown in Fig. 3(b) with a very prominent η peak. An unbinned maximum likelihood fit to the $M(\pi^0\pi^0\pi^0)$ distribution is performed, where the signal is modeled by the MC simulated shape convolved with a Gaussian resolution function, and the background contribution is described with a second-order Chebyshev polynomial function. The background fraction is estimated to be 0.3%, which is consistent with that found with the inclusive MC sample of 10 billion J/ψ events. We therefore neglect the background contribution in the extraction of the matrix elements.

As described in Sec. I, the conventional leading-order parametrization for $\eta \to \pi^0\pi^0\pi^0$ only relies on the quadratic slope parameter α. Analogous to the measurement for $\eta \to \pi^+\pi^-\pi^0$, an unbinned maximum likelihood fit to data is performed on the Z distribution as a function of $Z = X^2 + Y^2$ to extract the slope parameter. After taking into
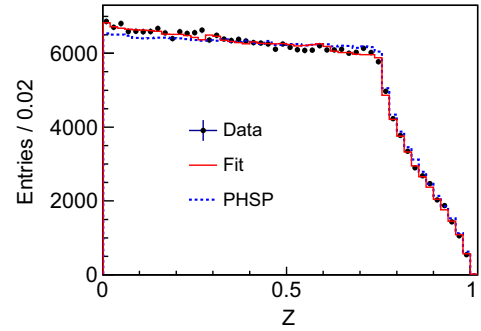

FIG. 4. Distribution of the kinematic variable Z for $\eta \to \pi^0\pi^0\pi^0$ candidates obtained from data (dots with error bars), PHSP-distributed MC events (dotted histogram), and the fit projection (solid histogram).

account the mass resolution and the detection efficiency, which are obtained from the MC simulation, the fit only considering the slope parameter up to Z term in Eq. (4) gives

$$\alpha = -0.0406 \pm 0.0035, \qquad (12)$$

where the uncertainty is statistical only. The fit result, as illustrated in Fig. 4, indicates that the decay amplitude with the quadratic slope parameter α describes data well. To directly compare with the previous BESIII measurement [12], $-0.055 \pm 0.014 \pm 0.004$, an alternative fit with the requirement $Z < 0.7$ is also performed and yields $\alpha = -0.046 \pm 0.005$, which is consistent with the previous measurement within uncertainties.

To test for higher-order contributions, an alternative fit including the terms $2\alpha Z + 2\beta(3X^2Y - Y^3)$ gives $\alpha = -0.0421 \pm 0.0037$ and $\beta = 0.0038 \pm 0.0033$, which implies that β is consistent with zero and this extra term has little impact on the value of α. Please note that one $\eta \to \pi^0\pi^0\pi^0$ event contributes to six entries in the Dalitz plot of X and Y, the parameter errors from this fit are multiplied by the factor of $\sqrt{6}$ to reflect the actual experimental statistics. We also perform the fits by including the terms $2\alpha Z + 2\gamma Z^2$ and find that $\gamma = -0.018 \pm 0.014$ is also consistent with zero, but has a large impact on α due to a strong correlation, -0.964, between α and γ. Therefore, with the current sample size, it is justified to ignore the higher-order contributions.

To search for the cusp effect near the $\pi^+\pi^-$ mass threshold, we evaluate the ratio of the experimental $\pi^0\pi^0$ invariant-mass distribution to the PHSP-distributed MC sample, as depicted in Fig. 5. No obvious structure around the $\pi^+\pi^-$ mass threshold is observed. Using the same approach as described in Ref. [13], which is also similar to NREFT [4], the cusp structure is parametrized in terms of the density function as $\rho(s_i) = \Re\sqrt{1 - s_i/4m_{\pi^\pm}^2}$, where $\Re$ is the real part, $i = 1, 2, 3$ denotes the three π^0's, and $s_i = (p_\eta - p_i)^2$ with $p_i^2 = m_i^2$. Here p_η and p_i are the four-momenta of the η and the ith π^0, respectively, while m_i is the π^0 invariant mass. For $s \geq 4m_{\pi^\pm}^2$, $\rho(s) = 0$. Then the amplitude squared is given by

$$|A|^2 \propto 1 + 2\alpha Z + 2\delta \sum_{i=1}^{3} \rho(s_i), \qquad (13)$$

where the factor of 2 in front of the cusp term δ is added to be consistent with the Z term. An unbinned maximum likelihood fit to data on the Z and $\sum_{i=1}^{3} \rho(s_i)$ distributions yields the following parameters

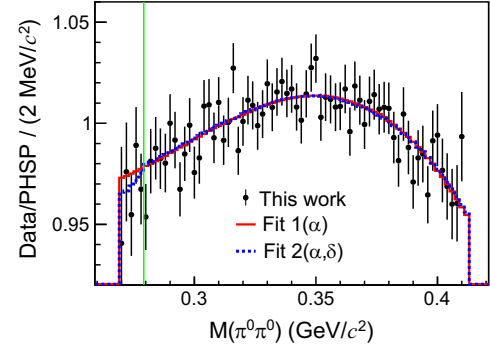$$\alpha = -0.0397 \pm 0.0036, \qquad \delta = -0.018 \pm 0.022, \qquad (14)$$

FIG. 5. Ratio between the experimental $\pi^0\pi^0$ invariant mass distributions (the black dots with error bars) or the fit results (colored curves) and the PHSP simulated distributions. The Fit $1(\alpha)$ and Fit $2(\alpha, \delta)$ correspond to the fit projections based on the results in Eq. (12) and Eq. (14), respectively. The vertical line corresponds to the $\pi^+\pi^-$ mass threshold.

where the uncertainties are statistical only. The correlation coefficient between α and δ is -0.304. The fitted value for δ is consistent with zero within the statistical uncertainty and the parameter α is almost unchanged, which indicates there is no evidence for a significant cusp effect in $\eta \to \pi^0\pi^0\pi^0$ decays. Comparing the log-likelihood values and the number of degrees of freedom of the fits with (α, δ) and α only, the statistical significance for nonzero δ is determined to be 0.8σ. The fit result is also illustrated in Fig. 5.

V. SYSTEMATIC UNCERTAINTIES

Various sources of systematic uncertainties on the measured Dalitz plot matrix elements have been investigated, including tracking efficiency, π^0 reconstruction, kinematic fit, efficiency binning, fit bias, and different resolution between data and MC simulation. For $\eta \to \pi^0\pi^0\pi^0$ candidates, an additional uncertainty due to the photon miscombination is also considered.

Differences between the data and MC samples for the tracking efficiency of charged pions are investigated using a control sample of $J/\psi \to \pi^+\pi^-\pi^0$ events. A transverse momentum and $\cos\theta$ dependent correction to the detection efficiency is obtained by comparing the efficiency between the data and MC simulation, where θ is the polar angle of the track. Similarly, a momentum dependent correction for π^0 reconstruction is investigated using $J/\psi \to \pi^+\pi^-\pi^0$ decays. Alternative fits are performed by considering the efficiency corrections for charged pions or π^0, and the changes of the matrix elements with respect to the nominal results are taken as the systematic uncertainties.

Uncertainties associated with the kinematic fits mainly come from the inconsistency of the track helix parameters and photon resolution between data and MC simulation. For $\eta \to \pi^+\pi^-\pi^0$, the helix parameters and error matrix for the charged tracks in the MC samples are corrected to eliminate the inconsistency between data and MC

simulation. While for $\eta \to \pi^0\pi^0\pi^0$ candidates, the raw photon energy from the EMC and the uncertainty of the photon energy in the kinematic fit are adjusted to reduce the difference between data and MC simulation. Alternative fits are performed with the corrected MC samples, and the corresponding differences on the matrix elements are taken as the systematic uncertainties.

Different binning schemes of the efficiency are exploited to estimate the associated uncertainties. The changes of the matrix elements with respect to the default fit results are assigned as the systematic uncertainties.

To estimate the systematic uncertainties due to the fitting procedure, input-output checks are performed with the dedicated MC samples. The deviations of the pull distributions from the standard normal distributions are taken as the systematic uncertainties.

The possible miscombination of photons in the $\eta \to \pi^0\pi^0\pi^0$ sample has been studied by matching the generated photon pairs to the selected π^0 candidates. The fraction of events with miscombined photons is determined to be 5.3%. Alternative fits to the dedicated $\eta \to \pi^0\pi^0\pi^0$ MC sample are performed with and without removing the miscombined events individually. The difference between the two fitting results is considered as a source of systematic uncertainty.

To evaluate the impact from the different resolutions of Dalitz plot variables between data and MC samples, alternative fits are performed by varying the resolution $\pm 10\%$. The changes of the matrix elements with respect to the default fit results are assigned as the systematic uncertainties. The impact from the background contribution is also checked and the change of the results is found to be negligible.

All of the above contributions are summarized in Table I, where the total systematic uncertainties are given by the quadratic sum of the individual uncertainties, assuming all the sources are independent.

For the measurement of the asymmetries in the $\eta \to \pi^+\pi^-\pi^0$ Dalitz plot, the systematic uncertainties are mainly

from the kinematic fit and the difference of tracking efficiency and π^0 reconstruction efficiency between data and MC simulation, as summarized in Table I. To estimate the uncertainties associated with the kinematic fit, the track helix parameters and error matrix of MC simulation are first corrected to reduce the difference between data and MC simulation. The efficiencies are then re-estimated with the corrected MC samples, and the differences on the asymmetries are taken as the systematic uncertainties. With the same method described above, the differences between data and MC samples for the tracking efficiency of charged pions and π^0 reconstruction are considered in the estimation of the efficiencies, and the differences in the asymmetries are taken as the systematic uncertainties.

VI. SUMMARY

Using a sample of $(10087 \pm 44) \times 10^6$ J/ψ decays collected by the BESIII detector, very clean samples of $631,686$ $\eta \to \pi^+\pi^-\pi^0$ events and $272,322$ $\eta \to \pi^0\pi^0\pi^0$ events are selected from $J/\psi \to \gamma\eta$ radiative decays. The matrix elements for the decays $\eta \to \pi^+\pi^-\pi^0$ and $\eta \to \pi^0\pi^0\pi^0$ have been determined precisely, and supersede the previous BESIII measurement [12], which is based on a subsample of the present data.

Including only the charge conjugation invariant terms from Eq. (2), the Dalitz plot matrix elements for $\eta \to \pi^+\pi^-\pi^0$ are determined to be

$$a = -1.097 \pm 0.005 \pm 0.001,$$
$$b = 0.158 \pm 0.006 \pm 0.003,$$
$$d = 0.070 \pm 0.006 \pm 0.001,$$
$$f = 0.134 \pm 0.010 \pm 0.003, \tag{15}$$

where the first uncertainties are statistical and the second systematic, here and in the following. Including the cubic term gX^2Y results in the following matrix elements

TABLE I. Relative systematic uncertainties of the matrix elements for $\eta \to \pi^+\pi^-\pi^0$ and $\eta \to \pi^0\pi^0\pi^0$ decays, and the Dalitz plot asymmetries for $\eta \to \pi^+\pi^-\pi^0$ decays (all values are given in %).

| Source	Results in Eq. (7)				Results in Eq. (9)								
	a	b	d	f	a	b	d	f	g	α	A_{LR}	A_Q	A_S
Tracking efficiency	0.01	0.02	0.12	0.02	0.01	0.04	0.01	0.02	0.02	$\cdots$	0.07	0.08	0.07
π^0 efficiency	0.03	0.18	0.08	0.07	0.02	0.13	0.01	0.04	0.16	0.23	0.01	0.18	0.13
Kinematic fit	0.07	2.06	0.14	1.96	0.06	1.98	0.18	2.29	0.57	0.01	0.73	32.3	12.7
Efficiency binning	0.04	0.29	0.42	0.11	0.01	0.33	0.76	0.53	3.04	0.15	$\cdots$	$\cdots$	$\cdots$
Fit bias	0.02	0.65	1.06	0.90	0.02	0.13	0.17	0.17	3.50	1.80	$\cdots$	$\cdots$	$\cdots$
Resolution	0.01	0.08	0.09	0.02	0.01	0.03	0.01	0.01	0.09	0.02	$\cdots$	$\cdots$	$\cdots$
Photon mis-combination	$\cdots$	$\cdots$	$\cdots$	$\cdots$	$\cdots$	$\cdots$	$\cdots$	$\cdots$	$\cdots$	0.75	$\cdots$	$\cdots$	$\cdots$
Total	0.09	2.19	1.16	2.16	0.07	2.02	0.80	2.36	4.67	1.97	0.74	32.3	12.8
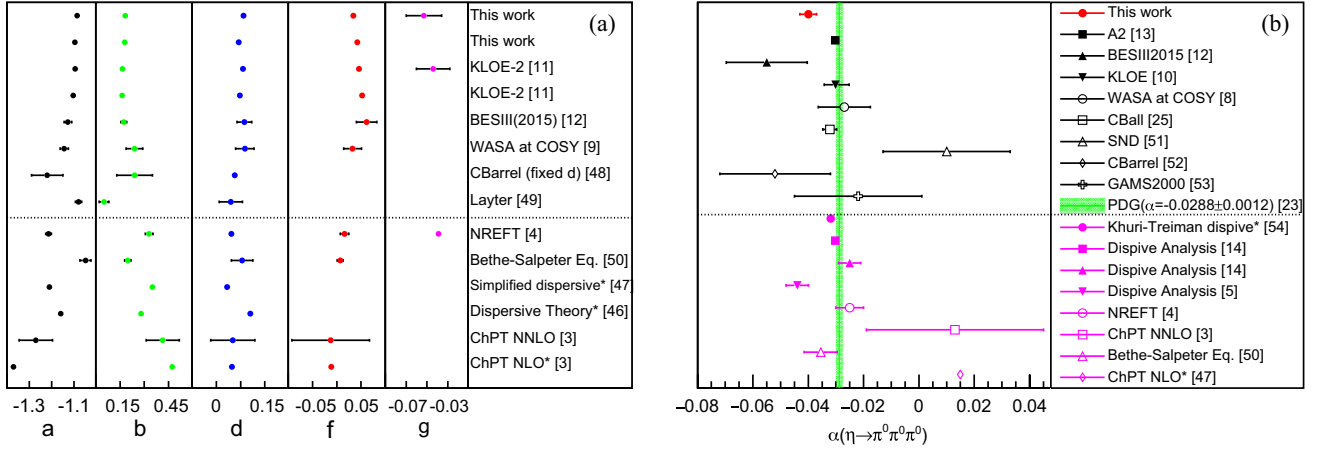
FIG. 6. Comparison of the experimental measurements and theoretical calculations for (a) $\eta \to \pi^+\pi^-\pi^0$ and (b) $\eta \to \pi^0\pi^0\pi^0$. No uncertainties were reported for theoretical predictions marked by $*$ in the legend.

$$a = -1.086 \pm 0.006 \pm 0.001,$$
$$b = 0.162 \pm 0.006 \pm 0.003,$$
$$d = 0.083 \pm 0.007 \pm 0.001,$$
$$f = 0.118 \pm 0.011 \pm 0.003,$$
$$g = -0.053 \pm 0.017 \pm 0.003. \qquad (16)$$

Our results are consistent with recent experimental results [9,11,12], and are in reasonable agreement with the theoretical calculation based on the dispersive approach and ChPT at next-to-next-to-leading order (NNLO) level [3,4,46,47], as summarized in Fig. 6(a).

Charge conjugation invariance in $\eta \to \pi^+\pi^-\pi^0$ is investigated by performing an alternative fit with odd powers of X (c and e) left free and checking the integrated asymmetries of the Dalitz plot distribution. The obtained values, $A_{LR} = (0.114 \pm 0.131 \pm 0.001)\%$, $A_Q = (-0.035 \pm 0.131 \pm 0.011)\%$ and $A_S = (-0.070 \pm 0.131 \pm 0.009)\%$, are consistent with zero and indicate no evidence for significant charge symmetry breaking. Comparison of the experimental asymmetries results are summarized in Table II. In addition, the higher order contributions $hXY^2 + lX^3$ are also checked, but no significant contribution is found.

The slope parameter for $\eta \to \pi^0\pi^0\pi^0$ is determined to be $\alpha = -0.0406 \pm 0.0035 \pm 0.0008$, which is consistent with the A2 measurement [13], $-0.0302 \pm 0.0008(\text{stat.})$,

within 2.8σ. The A2's result is the most precise measurement and from the fit with α as the only free paramter. Comparison between the theoretical calculations and experimental measurements of the slope parameters are shown in Fig. 6(b). No significant higher-order contribution is found at the current level of precision. In addition, the cusp effect in $\eta \to \pi^0\pi^0\pi^0$ is also investigated, but no obvious contribution is found.

ACKNOWLEDGMENTS

TABLE II. Experimental asymmetries in the Dalitz plot of $\eta \to \pi^+\pi^-\pi^0$ decays.

Experiment	$A_{LR}(\%)$	$A_Q(\%)$	$A_S(\%)$
This work	$0.114 \pm 0.131 \pm 0.001$	$-0.035 \pm 0.131 \pm 0.011$	$-0.070 \pm 0.131 \pm 0.009$
KLOE-2 [11]	$-0.050 \pm 0.045^{+0.050}_{-0.110}$	$0.018 \pm 0.045^{+0.048}_{-0.023}$	$0.004 \pm 0.045^{+0.031}_{-0.035}$
Jane [40]	0.28 ± 0.26	-0.30 ± 0.25	0.20 ± 0.25
Layter [24]	-0.05 ± 0.22	-0.07 ± 0.22	0.10 ± 0.22
Gormley [41]	1.5 ± 0.5	$\cdots$	0.5 ± 0.5

APPENDIX: ACCEPTANCE CORRECTED DATA

In order to directly taken as input for theoretical calculations, the tables containing Dalitz plot acceptance corrected data and the corresponding statistical uncertainties are provided in the HEPData database. To ensure that the results obtained from the acceptance data are consistent with those from the unbinned likelihood fit in this analysis, we also performed alternative fits with the least square method.

The Dalitz plot matrix elements for $\eta \to \pi^+\pi^-\pi^0$ and $\eta \to \pi^0\pi^0\pi^0$ are extracted from a fit to the acceptance corrected data by minimizing

$$\chi^2 = \sum_{i=1}^{X_{\text{bin}}} \sum_{j=1}^{Y_{\text{bin}}} \left(\frac{N_{ij}^{\text{cor}} - N_{\text{the}}^{ij}}{\sigma_{ij}}\right)^2 \quad \text{(A1)}$$

where the sum runs over all the bins and $N_{\text{the}}^{ij} = \int\int |A(X,Y)|^2 dX_i dY_j$. The acceptance corrected signal content in each bin of the Dalitz plot N_{ij}^{cor} is obtained by dividing event number, N_{ij}, by the corresponding acceptance, ε_{ij}. The acceptance is obtained from the signal MC in that bin. The statistical uncertainty σ_{ij} includes contributions from the experimental data and the efficiency.

Ignoring the high-order term gX^2Y and imposing charge conjugation invariance, the Dalitz plot matrix elements

for $\eta \to \pi^+\pi^-\pi^0$ extracted from the acceptance corrected data are

$$a = -1.096 \pm 0.006,$$
$$b = 0.157 \pm 0.006,$$
$$d = 0.069 \pm 0.006,$$
$$f = 0.131 \pm 0.012, \quad \text{(A2)}$$

and the corresponding correlation matrix

$$\begin{pmatrix} & a & b & d & f \\ \hline a & 1.000 & -0.240 & -0.405 & -0.783 \\ b & & 1.000 & 0.323 & -0.292 \\ d & & & 1.000 & 0.107 \\ f & & & & 1.000 \end{pmatrix}. \quad \text{(A3)}$$

The uncertainties are statistical only, here and in the following. The results are consistent within statistical uncertainties with the values obtained using the unbinned maximum likelihood fit. Including the cubic term gX^2Y results in the following matrix elements

$$a = -1.085 \pm 0.007,$$
$$b = 0.162 \pm 0.007,$$
$$d = 0.083 \pm 0.008,$$
$$f = 0.114 \pm 0.013,$$
$$g = -0.056 \pm 0.019, \quad \text{(A4)}$$

and corresponding correlation matrix

$$\begin{pmatrix} & a & b & d & f & g \\ \hline a & 1.000 & -0.068 & 0.046 & -0.825 & -0.518 \\ b & & 1.000 & 0.401 & -0.362 & -0.251 \\ d & & & 1.000 & -0.181 & -0.615 \\ f & & & & 1.000 & 0.419 \\ g & & & & & 1.000 \end{pmatrix}. \quad \text{(A5)}$$

While the slope parameter for $\eta \to \pi^0\pi^0\pi^0$ is determined to be

$$\alpha = -0.0409 \pm 0.0038. \quad \text{(A6)}$$

Please note that one $\eta \to \pi^0\pi^0\pi^0$ event contributes to six entries in the Dalitz plot of X and Y, the parameter error from fitting to the $\eta \to \pi^0\pi^0\pi^0$ acceptance corrected data must be multiplied by the factor of $\sqrt{6}$ to reflect the actual experimental statistics.

[1] S. S. Fang, Natl. Sci. Rev. **8,** nwab052 (2021).
[2] J. Gasser and H. Leutwyler, Nucl. Phys. **B250,** 539 (1985).
[3] J. Bijnens and K. Ghorbani, J. High Energy Phys. 11 (2007) 030.
[4] S. P. Schneider, B. Kubis, and C. Ditsche, J. High Energy Phys. 02 (2011) 028.
[5] K. Kampf, M. Knecht, J. Novotny, and M. Zdrahal, Phys. Rev. D **84,** 114015 (2011).
[6] P. Guo, I. V. Danilkin, D. Schott, C. Fernández-Ramírez, V. Mathieu, and A. P. Szczepaniak, Phys. Rev. D **92,** 054016 (2015).
[7] G. Colangelo, S. Lanz, H. Leutwyler, and E. Passemar, Eur. Phys. J. C **78,** 947 (2018).
[8] C. Adolph et al. (WASA-at-COSY Collaboration), Phys. Lett. B **677,** 24 (2009).
[9] P. Adlarson et al. (WASA-at-COSY Collaboration), Phys. Rev. C **90,** 045207 (2014).
[10] F. Ambrosino et al. (KLOE Collaboration), Phys. Lett. B **694,** 16 (2011).
[11] A. Anastasi et al. (KLOE-2 Collaboration), J. High Energy Phys. 05 (2016) 019.
[12] M. Ablikim et al. (BESIII Collaboration), Phys. Rev. D **92,** 012014 (2015).
[13] S. Prakhov et al. (A2 Collaboration), Phys. Rev. C **97,** 065203 (2018).
[14] G. Colangelo, S. Lanz, H. Leutwyler, and E. Passemar, Phys. Rev. Lett. **118,** 022001 (2017).
[15] P. Guo, I. V. Danilkin, C. Fernández-Ramírez, V. Mathieu, and A. P. Szczepaniak, Phys. Lett. B **771,** 497 (2017).
[16] C. O. Gullstrom, A. Kupsc, and A. Rusetsky, Phys. Rev. C **79,** 028201 (2009).
[17] M. Bissegger, A. Fuhrer, J. Gasser, B. Kubis, and A. Rusetsky, Phys. Lett. B **659,** 576 (2008).
[18] P. Budini and L. Fonda, Phys. Rev. Lett. **6,** 419 (1961).
[19] J. R. Batley et al. (NA48/2 Collaboration), Phys. Lett. B **633,** 173 (2006).
[20] M. Ablikim et al. (BESIII Collaboration), Phys. Rev. Lett. **130,** 081901 (2023).
[21] B. Kubis and S. P. Schneider, Eur. Phys. J. C **62,** 511 (2009).
[22] M. Ablikim et al. (BESIII Collaboration), Chin. Phys. C **46,** 074001 (2022).
[23] R. L. Workman et al. (Particle Data Group), Prog. Theor. Exp. Phys. **2022,** 083C01 (2022).
[24] J. G. Layter, J. A. Appel, A. Kotlewski, W. Y. Lee, S. Stein, and J. J. Thaler, Phys. Rev. Lett. **29,** 316 (1972).
[25] S. Prakhov et al. (Crystal Ball Collaboration), Phys. Rev. C **79,** 035204 (2009).
[26] M. Ablikim et al. (BESIII Collaboration), Nucl. Instrum. Methods Phys. Res., Sect. A **614,** 345 (2010).
[27] C. H. Yu et al., Proceedings of IPAC2016, Busan, Korea (2016), 10.18429/JACoW-IPAC2016-TUYA01.
[28] M. Ablikim et al. (BESIII Collaboration), Chin. Phys. C **44,** 040001 (2020).
[29] K. X. Huang, Z. J. Li, Z. Qian, J. Zhu, H. Y. Li, Y. M. Zhang, S. S. Sun, and Z. Y. You, Nucl. Sci. Tech. **33,** 142 (2022).
[30] X. Li et al., Radiat. Detect. Technol. Methods **1,** 13 (2017).
[31] P. Cao et al., Nucl. Instrum. Methods Phys. Res., Sect. A **953,** 163053 (2020).
[32] S. Agostinelli et al., Nucl. Instrum. Methods Phys. Res., Sect. A **506,** 250 (2003).
[33] S. Jadach, B. F. L. Ward, and Z. Was, Phys. Rev. D **63,** 113009 (2001).
[34] S. Jadach, B. F. L. Ward, and Z. Was, Comput. Phys. Commun. **130,** 260 (2000).
[35] D. J. Lange, Nucl. Instrum. Methods Phys. Res., Sect. A **462,** 152 (2001).
[36] R. G. Ping, Chin. Phys. C **32,** 599 (2008).
[37] J. C. Chen, G. S. Huang, X. R. Qi, D. H. Zhang, and Y. S. Zhu, Phys. Rev. D **62,** 034003 (2000).
[38] R. L. Yang, R. G. Ping, and H. Chen, Chin. Phys. Lett. **31,** 061301 (2014).
[39] E. Richter-Was, Phys. Lett. B **303,** 163 (1993).
[40] M. R. Jane et al., Phys. Lett. **48B,** 260 (1974).
[41] M. Gormley, E. Hyman, W. Lee, T. Nash, J. Peoples, C. Schultz, and S. Stein, Phys. Rev. Lett. **21,** 402 (1968).
[42] F. Ambrosino et al. (KLOE Collaboration), J. High Energy Phys. 05 (2008) 006.
[43] S. Gardner and J. Shi, Phys. Rev. D **101,** 115038 (2020).
[44] H. Akdag, T. Isken, and B. Kubis, J. High Energy Phys. 02 (2022) 137; 12 (2022) 156.
[45] H. Akdag, B. Kubis, and A. Wirzba, arXiv:2212.07794.
[46] J. Kambor, C. Wiesendanger, and D. Wyler, Nucl. Phys. **B465,** 215 (1996).
[47] J. Bijnens and J. Gasser, Phys. Scr. T **99,** 34 (2002).
[48] A Abele et al. (Crystal Barrel Collaboration), Phys. Lett. B **417,** 197 (1998).
[49] J. G. Layter, J. A. Appel, A. Kotlewski, W. Y. Lee, S. Stein, and J. J. Thaler, Phys. Rev. D **7,** 2565 (1973).
[50] B. Borasoy and R. Nissler, Eur. Phys. J. A **26,** 383 (2005).
[51] M. N. Achasov et al. (SND Collaboration), JETP Lett. **73,** 451 (2001).
[52] A Abele et al. (Crystal Barrel Collaboration), Phys. Lett. B **417,** 193 (1998).
[53] D. Alde et al., Z. Phys. C **25,** 225 (1984).
[54] M. Albaladejo and B. Moussallam, Eur. Phys. J. C **77,** 508 (2017).